BBA - Bioenergetics 1859 (2018) 1039–1044

Contents lists available at ScienceDirect

BBA - Bioenergetics

journal homepage: www.elsevier.com/locate/bbabio

Desiccation tolerant lichens facilitate in vivo H/D isotope effect measurements in oxygenic photosynthesis

David J. Vinyard[a,b,1], Gennady M. Ananyev[a,b], G. Charles Dismukes[b,c,*]

[a] Department of Chemistry, Princeton University, Princeton, NJ 08544, USA
[b] Waksman Institute of Microbiology, Rutgers University, Piscataway, NJ 08854, USA
[c] Department of Chemistry and Chemical Biology, Rutgers University, Piscataway, NJ 08854, USA

ARTICLE INFO

Keywords:
Photosystem II
Lichens
Isotope effects
Water oxidation

ABSTRACT

We have used the desiccation-tolerant lichen *Flavoparmelia caperata*, containing the green algal photobiont *Trebouxia gelatinosa*, to examine H/D isotope effects in Photosystem II in vivo. Artifact-free H/D isotope effects on both PSII primary charge separation and water oxidation yields were determined as a function of flash rate from chlorophyll-*a* variable fluorescence yields. Intact lichens could be reversibly dehydrated/re-hydrated with H_2O/D_2O repeatedly without loss of O_2 evolution, unlike all isolated PSII preparations. Above a threshold flash rate, PSII charge separation decreases sharply in both D_2O and H_2O, reflecting loss of excitation migration and capture by PSII. Changes in H/D coordinates further slow charge separation in D_2O (−23% at 120 Hz), attributed to reoxidation of the primary acceptor Q_A^-. At intermediate flash rates (5–50 Hz) D_2O decreases water oxidation efficiency (O_2 evolution) by −2–5%. No significant isotopic difference is observed at slow flash rates (< 5 Hz) where charge recombination dominates. Slower D_2O diffusion, changes in hydrogen bonding networks, and shifts in the pK_a's of ionizable residues may all contribute to these systematic variations of H/D isotope effects. Lichens' reversible desiccation tolerance allows highly reproducible H/D exchange kinetics in PSII reactions to be studied in vivo for the first time.

1. Introduction

In oxygenic photosynthesis, the Photosystem II (PSII) reaction center acts as a solar-driven water-plastoquinone (PQ) oxidoreductase. The primary electron donor in PSII, P_{680}, contains chlorophyll-*a*. Upon excitation of P_{680}, a pheophytin (Pheo) cofactor is reduced and a metastable [$P_{680}^+Pheo^-$] charge separated pair is formed. Pheo reduces the primary PQ acceptor, Q_A, which reduces the secondary PQ acceptor, Q_B. On the donor side of PSII, the P_{680}^+ hole is reduced by a conserved tyrosine residue, Y_Z. Y_Z is reduced by the water oxidizing complex (WOC), which is a Mn_4CaO_5 inorganic cluster embedded in the protein structure. The WOC oxidizes two molecules of water to O_2 via four sequential one-electron oxidations coupled to proton losses. These redox intermediates are known as S_i-states (i = 0–4). Protons generated from water oxidation are released to the thylakoid lumen [1].

Despite decades of biochemical and biophysical experimentation and theory, the complete chemical mechanism of WOC-dependent O_2 evolution is not fully known [2–4]. Because water is both the substrate and the solvent, detailed experiments tracking individual species from substrate to product are complex and elusive [5].

The WOC is surrounded by several hydrogen-bonding networks that form channels for water, proton, and/or O_2 transport. The “narrow” channel extends from the O4 μ-oxo ligand of the WOC to the lumen and includes D1-D61 [6]. This channel has a low barrier for water transport [7] and may provide the substrate water during the S_2 to S_3 transition [8]. The “broad” channel extends from the “dangler” Mn4 of the OEC to the lumen and includes a high-affinity chloride ion [7, 9]. This channel has been proposed to support proton release from the WOC [10–12]. The “large” channel is the most extensive and least characterized network [9, 13]. The large channel has a moderate barrier for water transport [7] and likely serves this role [14]. If the S_2 to S_3 transition substrate water enters via the narrow channel, the S_4 to S_0 transition substrate water may enter through the large channel. Although O_2 in nonpolar, its transport from the WOC to the lumen likely utilizes hydrogen-bonding networks [15]. The large channel has been proposed to be both a water and O_2 transport network from both computational [15] and experimental [14] studies.

Kinetic isotope effects (KIE's) reflect differences in the zero point energies of the reactant(s) and transition states and have frequently been used to study PSII chemistry *in vitro*. However, the interpretation

* Corresponding author at: 610 Taylor Rd., Piscataway, NJ 08854, USA.
E-mail address: dismukes@chem.rutgers.edu (G.C. Dismukes).
[1] Current Address: Department of Biological Sciences, Louisiana State University, Baton Rouge, LA 70803 USA.

https://doi.org/10.1016/j.bbabio.2018.05.014
Received 28 February 2018; Received in revised form 21 May 2018; Accepted 23 May 2018
Available online 31 May 2018
0005-2728/

of KIE's in PSII is complicated by equilibrium isotope effects that alter the Boltzmann populations of configurational states, arising from various sources such as changes in hydrogen bonding networks [16] and shifts in the pK_a's of ionizable amino acid residues [17]. These issues are exasperated by variations in the properties of biochemically purified PSII compared to PSII in vivo, and by unintentional protein denaturation upon solvent water exchange. To overcome the latter two problems, we have used lichens to facilitate high fidelity *in vivo* measurements of PSII in the presence of either H_2O or D_2O.

Lichens are fungi-algae (or fungi-cyanobacteria) symbionts that have unique desiccation tolerance [18]. This evolutionary adaptation can be exploited in the laboratory to efficiently remove non-structural water and replace it with isotopically enriched water for isotope effect experiments. The reversible loss of PSII activity in lichens upon dehydration has been previously studied by chlorophyll variable fluorescence yield (F_v) and lifetime measurements and oximetry [19–23] from which it was established that energy transfer from the algal antenna system to the PSII reaction center is disrupted. Here we use F_v to measure both successful PSII charge separation ($[P^+Q_A^-]$ formation) and the yield of its downstream photochemical reaction, water oxidation (O_2 evolution), via the dependence of F_v [24].

2. Materials and methods

Flavoparmelia caperata, which contains the green algal photobiont *Trebouxia gelatinosa* [25], was collected from the bark of mature *Quercus rubrus* approximately one meter above the soil in Princeton, New Jersey. Species identification was confirmed using traditional "spot tests" on the lichen cortex and medulla which detect characteristic metabolites [26]. PSII in *Trebouxia gelatinosa* and all green algae contains a single D1 isoform and the extrinsic subunits PsbO, PsbP, and PsbQ [27, 28]. Thallus samples were stored for no more than one week under low light conditions at room temperature and 40–50% relative humidity. Before analysis, residual bark was removed from the thallus and a 6-mm diameter sample of natural thickness (approximately 100 μm) was cut from a terminal lobe (youngest portion).

For reversibility experiments (Fig. 1), a sample was mounted into the chamber of a homebuilt fast repetition rate (FRR) fluorometer [24]. For desiccation, a plastic conical tube containing a suspended cheesecloth bag of calcium sulfate was mounted over the sample chamber and sealed with silicone grease. For hydration, 50 μL of either ultra-pure H_2O (MilliQ) or 99.9 atom % D_2O (Sigma-Aldrich) was added to the lichen sample.

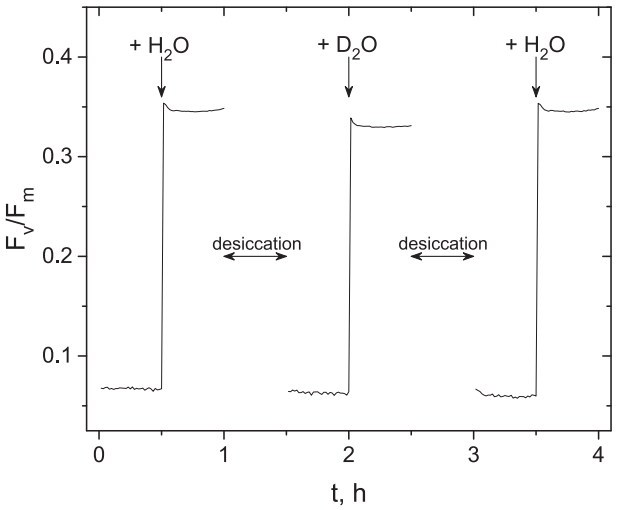

Fig. 1. Representative reversible desiccation and hydration cycling of *F. caperata*. A dried 6-mm diameter thallus sample was dark adapted for 2 min then subjected to 50 single turnover flashes at 5 Hz. This cycle was repeated for the timescales shown. At times indicated by vertical arrows, either 50 μL of H_2O or 50 μL D_2O was added to the sample. The sample was placed in a chamber containing calcium sulfate during the indicated desiccation periods.

For all other experiments, air-dried lichen samples were hydrated with 50 μL or H_2O or D_2O and incubated under room light for 10 min. Excess liquid was blotted with a laboratory tissue and a second 50 μL aliquot of H_2O or D_2O was added immediately prior to dark adaptation. For D_2O experiments, ^1H contamination of the D_2O pool surrounding the lichen sample was monitored using Fourier transform infrared spectroscopy-attenuated total reflectance (FTIR-ATR). O-H/O-D stretching frequencies were compared between fresh D_2O, fresh H_2O, and D_2O rinses after incubation with the lichen sample. This method indicated a maximum presence of 5% ^1H contamination (presumably as HDO) and is attributed to H_2O exchange with the lichen sample and absorption from humidity.

In a parallel study, water content in lichen samples was monitored using micro-gravimetry. At ambient relative humidity (46%) and 21 °C, water content decreased from approximately 2.1 to 0.05–0.10 (ratio of wet/dry wt.) over 2000 s (ten Velduis, Ananyev, and Dismukes, *submitted*). This value of residual water content is in agreement with FTIR-ATR measurements and likely represents tightly held structural water. Therefore, the enrichment of either H_2O or D_2O in our experiments is ≥90–95%.

FRR fluorescence measurements have been previously described [24]. Briefly, the instrument uses a laser diode excitation source (λ_{max} = 655 nm) at a maximal flash intensity of 32,000 μE m^{-2} s^{-1}. Resulting chlorophyll-*a* fluorescence is detected through a sharp edge filter (λ_{max} = 685 nm) by a large area avalanche photodiode before signal processing. Data are collected following a two-minute dark adaptation period to allow the metastable S_2 and S_3 states to decay to S_1. In each 50 μs single turnover flash, Q_A is fully reduced to Q_A^-. A sequence of 50 single turnover flashes is applied at a selected flash rate for each experiment. Following another two-minute dark adaptation, the 50-flash series is repeated. Data from approximately 120 measurements is ensemble averaged.

Oscillations in F_v/F_m, where $F_v = F_m - F_o$, were analytically fit to the VZAD model as previously described [29]. Alternatively, the Fourier transform of each data set was taken and the period determined by the maximum Fourier amplitude [29, 30].

3. Results

When field samples of *Flavoparmelia caperata* are desiccated in the laboratory, PSII charge separation yield (measured using variable chlorophyll-*a* fluorescence as F_v/F_m) approached zero (Fig. 1). Throughout, we normalize F_v to the total yield of chlorophyll fluorescence ($F_v + F_o = F_m$) to obtain the intensive quantity F_v/F_m which is proportional to the quantum yield of PSII charge separation, as first described by Duysens and Sweers [31]. Following the addition of H_2O to the lichen surface and absorption, PSII charge separation was restored within a two-minute dark adaption period between water addition and the first data point acquisition. F_v/F_m remained high during subsequent measurements. The sample was then desiccated for 30 min by incubation in a chamber containing calcium sulfate (0% relative humidity). Removal of non-structural water was confirmed by the return of the original low fluorescence signal. The same sample was then hydrated with D_2O, resulting in a slightly lower signal than that produced by H_2O hydration (F_v/F_m = 0.347 ± 0.002 for H_2O and 0.331 ± 0.002 and D_2O). Following another desiccation treatment, H_2O was added to the same sample and activity was restored to the initial H_2O level (F_v/F_m = 0.347 ± 0.003). Provided the flash frequency is ≤10 Hz, the lichen sample does not initiate photo-protective mechanisms and the experimental result shown in Fig. 1 can be repeated at least three times on the same sample without measurable changes.

FRR fluorometry allows variable chlorophyll-*a* fluorescence to be

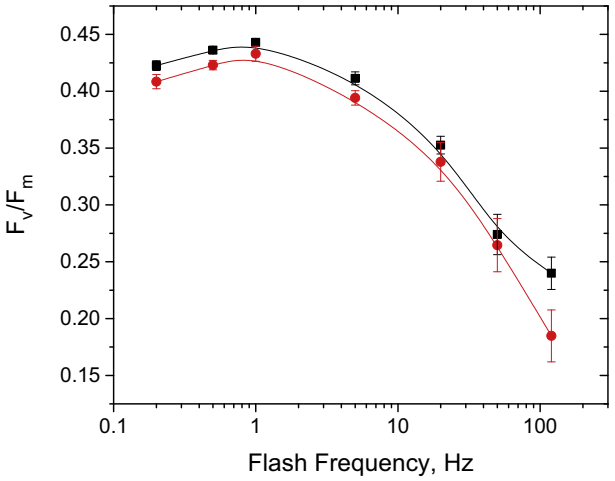

Fig. 2. Average charge separation yield (F_v/F_m) in *F. caperata* as a function of flash frequency when hydrated with H_2O (black) or D_2O (red). The average F_v/F_m level reflects the primary charge separation quantum yield ($[P^+Q_A^-]$ formation). Data represent the means ± standard errors of 50 sequential flashes, each following 2 min of dark adaption. Raw data are shown in Fig. S1.

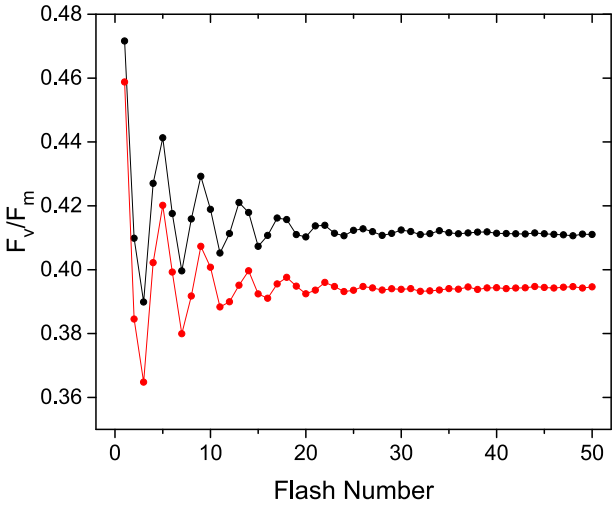

Fig. 3. Single turnover flashes induce oscillations in F_v/F_m in *F. caperata* at 5 Hz when hydrated with H_2O (black) or D_2O (red) following 2 min of dark adaptation. Samples are identical. Data for other flash frequencies is shown in Fig. S1.

studied over a wide range of flash frequencies. The dark times between single turnover flashes were varied from 8.5 to 5000 ms corresponding to flash rates of 120 to 0.2 Hz, respectively. As shown in Fig. 2, average F_v/F_m values of lichen samples hydrated in H_2O reach a maximum at 1 Hz flash rate and drop sharply above this flash rate, decreasing by 40% at 120 Hz. Lichens exhibit less charge separation capacity than free-living algae and have the earliest onset and steepest decrease in charge separation yield with flash rate of any phototroph that we have examined [32]. Average F_v/F_m values of lichen samples dehydrated then rehydrated in D_2O follow the same trend, but are uniformly lower than in H_2O by a small amount (≤5%) from 0.2 to 50 Hz. Above 50 Hz this difference increases substantially to approximately 23% lower at 120 Hz in D_2O vs. H_2O. At this high flash frequency, PSII acceptor side kinetics limit charge separation and the large observed H/D isotope effect indicates that H/D coordinates are specifically involved in these acceptor reactions.

Because the lichen sample was dark adapted for 2 min before each FRR fluorescence measurement, the S_1 intermediate of the WOC was highly populated [33]. Application of a train of short (single turnover) flashes reveals that F_v/F_m oscillates with a damped period-four flash pattern that reflects the efficiency of the primary charge separation reaction going on to complete the water oxidizing cycle [24]. These oscillations at 5 Hz flash rate are shown in Fig. 3 and data for all frequencies tested are shown in Fig. S1. Loss of period-four oscillation amplitude during the flash train reveals the equilibration of the populations of the four S-state intermediates and can be fitted to standard models.

In Fig. 3, not only is the steady-state F_v/F_m level lower in D_2O vs. H_2O by 5%, but the oscillations damp more quickly. The data were analytically fit to the VZAD model to quantify water oxidation efficiency (Fig. 4A) as previously described [29]. The Kok miss parameter (α) is generally larger in D_2O vs. H_2O (Fig. 4B), while double hits (β) and backward transitions (δ) show no significant differences (Fig. 4C and D). The difference in misses is greatest at 20 Hz and 5 Hz (26% and 32% higher in D_2O vs. H_2O, respectively). Inactivation events (ε) were negligible in both H_2O and D_2O.

The net efficiency of water oxidation can be represented simply by the hit parameter (γ), which is defined as $\gamma = 1 - \alpha - \beta - \delta/2 - \varepsilon/4$, where the four inefficiency parameters are defined in the VZAD cycle (Fig. 4A). The hit probability is the fraction of charge separation events in which the S-state cycle advances exactly one step forward towards O_2 evolution. As shown in Fig. 5A, hits mirror the miss data and are significantly higher in H_2O vs. D_2O, peaking between 20 and 5 Hz, and decreasing to zero difference at both lower and higher flash frequencies.

While the hit parameter is derived from a fitted analytical model, oscillations in F_v/F_m can be quantified directly by simple model-independent Fourier transformation of the oscillations [29, 30]. For a perfect water oxidation complex without damping of oscillations, the period would be exactly 4 (1/Period = 0.25 WOC cycles per flash). As shown in Fig. 5B, the inverse period is significantly lower than 0.25 at all flash frequencies studied. The Fourier transform period follows a similar isotopic trend as the VZAD model hit data at high flash rates, decreasing sharply above 50 Hz. By contrast, the Fourier transform period retains a significant isotopic difference at the lower flash rates (< 20 Hz) where substrate water diffusion and charge recombination contribute to the cycle period.

4. Discussion

At the lowest flash rate used in this work (0.2 Hz), the long spacing between flashes (5 s) is much slower than the limiting rates of either WOC cycling or acceptor side electron and proton transfer. By contrast, at the highest flash rate (120 Hz, 8.5 ms between flashes) F_v/F_m becomes more sensitive to D_2O exchange as successive transfers of electrons from Q_A^- to Q_B and protons from the surrounding medium to form Q_BH_2 become rate-limiting. This result is consistent with the observed ~10 ms halftime for PQ/PQH_2 exchange at the Q_B site [34]. At this kinetic regime, the yield of $[P_{680}^+Q_A^-]$ formation following a single turnover flash is decreased because a larger fraction of reaction centers is closed (Q_A^- has not reoxidized from the prior flash). The large change in F_v/F_m in H_2O vs. D_2O (23%) indicates that H/D coordinates change during PQ electron transfer and/or exchange.

At intermediate flash frequencies (0.5–50 Hz, 2 s–20 ms between flashes, respectively), the kinetics of WOC cycling approach the time between flashes. By summing the rates of individually measured S-state transitions, the upper limit of O_2 production by the WOC is 1.3–2.1 ms. However, both steady-state and single turnover flash experiments show that observed halftimes for O_2 production are on the order of 11–40 ms [27]. The magnitude of H/D isotope dependence is highest at 5 Hz (20 ms between flashes). At this frequency, D_2O results in a 32% increase in misses (Fig. 4B), a 3.4% decrease in hits (Fig. 5A), and a 2.2% decrease in 1/Period (Fig. 5B). At this intermediate flash frequency, the fraction of charge separation events that go on to do productive water

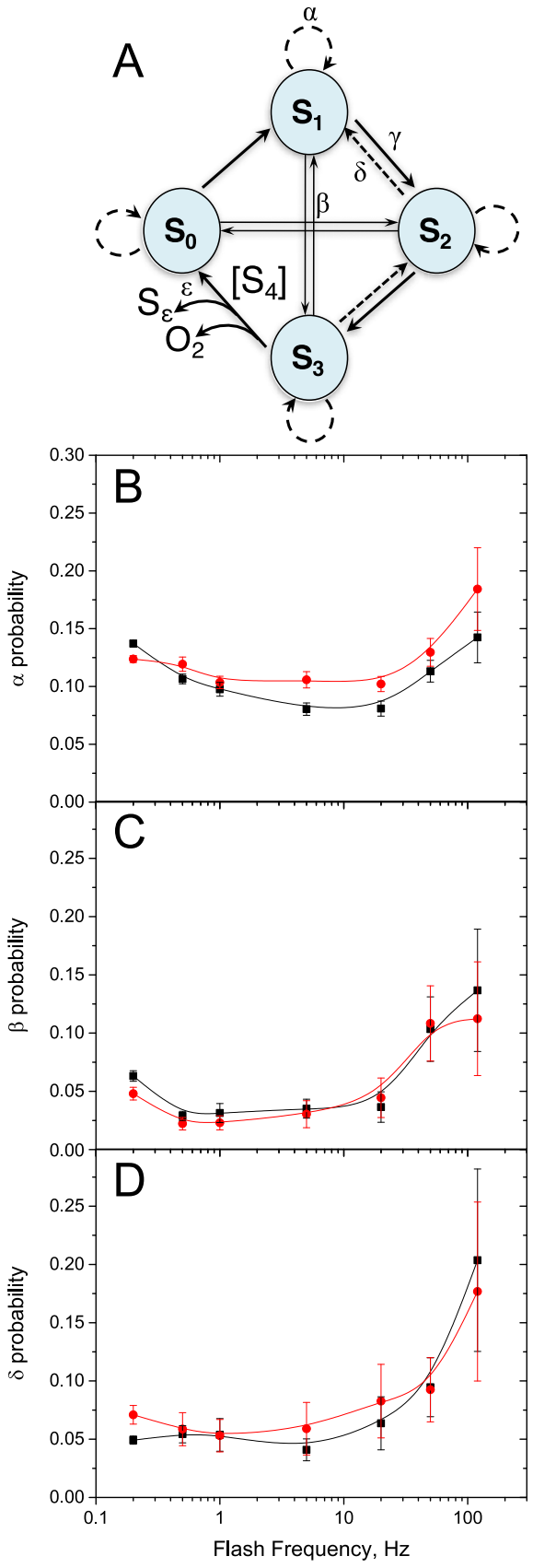

Fig. 4. Water oxidation efficiency was quantified by fitting oscillations in F_v/F_m to the VZAD analytical model [29] (panel A). This model includes misses (α, panel B), double hits (β, panel C), and backward transitions (δ, panel C). All inactivation event (ε) values were either 0 or ≤0.001. Data from *F. caperata* samples hydrated with H_2O are shown in black and with D_2O in red. Data represent best fits ± standard error (reflecting uniqueness of fit).

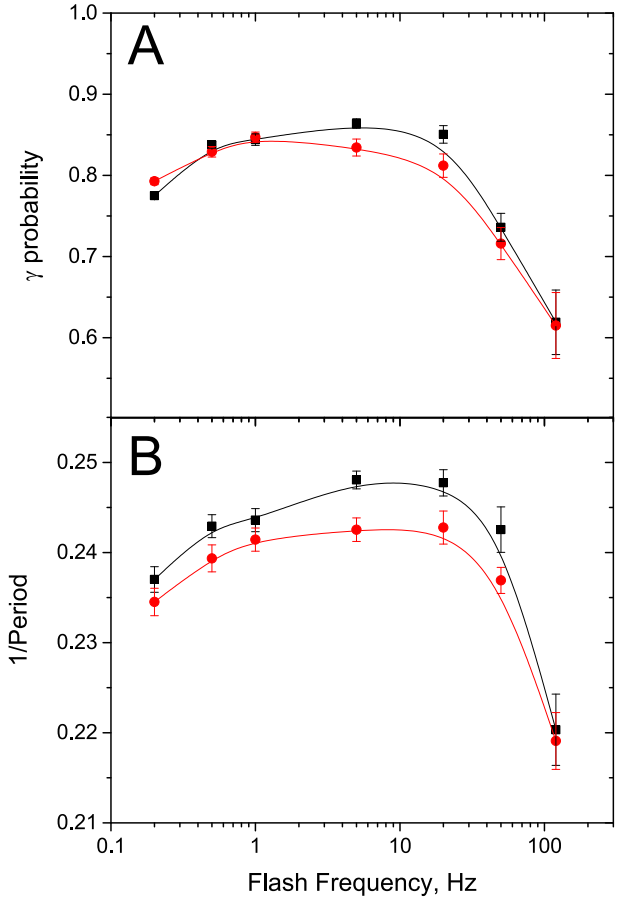

Fig. 5. Net water oxidation efficiency in *F. caperata* when hydrated with H_2O (black) or D_2O (red). The VZAD model hit parameter (γ) is shown in panel A. Model-independent periodicity from the Fourier transform of the oscillations is shown in panel B. Data represent best fits ± standard error (reflecting uniqueness of fit).

oxidation exhibit a significantly larger H/D isotope dependence than those at very slow or very fast flash frequencies. The changes may reflect fractionation arising from substrate water diffusion or H/D coordinates in the WOC environment that affect hydrogen bonding networks and/or the pK_a's of titratable groups.

An increase in the miss parameter in the presence of D_2O was previously reported by Junge and coworkers in isolated higher plant thylakoids (1997). At a 1 Hz flash frequency, misses were 9% in H_2O and 14% in D_2O [35]. However, when PSII core complexes were analyzed at 10 Hz, misses were higher (20%) and no difference was observed between H_2O and D_2O [35]. Such sample dependence highlights the need for robust *in vitro* methods to study isotope effects free from artifacts.

The H/D effects observed here likely also reflect the physical differences between the transport of H_2O and D_2O. Given D_2O's higher density ($\rho = 1.044\ g\ mL^{-1}$) and much larger viscosity (22% larger $\eta = 1.115$ mPa s) at 25° compared to H_2O ($\rho = 0.9971\ g\ mL^{-1}$ and $\eta = 0.890$ mPa s) [17], both kinematic (mass of the water molecule) and frictional drag (medium resistance) contribute, but with the latter making the dominant influence in slowing diffusion and hydrostatic flow. Hence, it is not surprising that water diffusion through the PSII protein matrix leading to O_2 production and proton transfer to Q_B would be altered by H/D exchange of the solvent. Within cells, perhaps the most important consideration is the resulting change in diffusivity which is dominated by the change in frictional drag. The self-diffusion coefficient of D_2O is 18.6% less than that of H_2O ($D = 2.229 \times 10^{-5}\ cm^2\ s^{-1}$ in H_2O vs. $1.872 \times 10^{-5}\ cm^2\ s^{-1}$ in D_2O) [36]. The magnitude of this difference is similar to that of the change in

the miss parameter at intermediate flash frequencies, confirming that diffusive water transport alone is sufficient to account for the magnitude of the observed effects. Actual water diffusion within channels of the PSII complex is an area of active study (see Introduction section and [16, 37]). Further tests of this hypothesis could be examined by investigating the consequences of H_2O/D_2O exchange at lower water content where the water chemical potential (osmotic pressure) increases. Theory predicts that flow of water under control of osmotic pressure can greatly exceed diffusive flow, for example by 10-fold in the case of red blood cells [38].

The kinetics and thermodynamics of proton release are also affected by D_2O exchange. Differences in the bond energies of O—H and O—D [39] are reflected in the slightly higher activation energy for D_2O oxidation by PSII as reported by Renger and coworkers (143 kJ mol^{-1} vs. 140 kJ mol^{-1} for H_2O) [40]. The introduction of D_2O also alters and stabilizes hydrogen bonding networks in PSII, and shifts in the pK_a's of ionizable residues. Indeed, H/D KIE's in PSII are pH-dependent and largest in steps that involve proton transfer. For example, the $S_2 \rightarrow S_3$ transition ($t_{1/2}$ = 180–460 μs) is most affected in D_2O producing k_H/k_D values of 1.3 to 2.4 depending on PSII sample preparation [35, 41, 42]. This KIE likely has contributions from the aforementioned solvent frictional drag, higher bond energy, and reduced deuteron conduction. Although we are restricted by the decreasing yield of charge separation in lichens to slow flash rates, we do see the solvent isotope effect discontinuously increases at 120 Hz flash rate reaching 23% (Fig. 2). We suggest this abrupt increase likely reflects the onset of an additional contribution to the solvent isotope effects observed at lower flash rates that we have already attributed to differences in water diffusivity and H/D-O bond energies. The additional contribution to solvent H/D isotope fractionation above this flash rate likely have contributions from proton transport kinetics on the acceptor side of PSII.

The hydrogen-bonding environment surrounding the WOC facilitates water delivery and proton release as reviewed in [16]. Recently, measurements of O_2 release kinetics from *in vitro* PSII preparations have been used to probe changes in these hydrogen-bonding networks as a result of point mutations [43, 44] or D_2O exchange [45]. However, work in our laboratory has shown that O_2 released by the algal symbionts in lichens is partially consumed by respiration in fungal cells (ten Velduis, Ananyev, and Dismukes, *submitted*). Therefore, *in vivo* studies on lichens are well suited for variable chlorophyll-*a* fluorescence methods and not oximetry.

In conclusion, lichens provide a robust and reversible system for observing H/D isotope fractionation of the primary charge separation reaction and subsequent coupled reactions of oxygenic photosynthesis in living cells without need biochemical extraction. By monitoring chlorophyll-*a* variable fluorescence as a function of flash frequency, kinetic regimes were identified where H/D effects on either the PSII acceptor or donor sides were observed. Future studies on the H/D kinetic isotope effects of individual WOC S-states are feasible and will be the subject of future work.

Supplementary data to this article can be found online at https://doi.org/10.1016/j.bbabio.2018.05.014.

Transparency document

The http://dx.doi.org/10.1016/j.bbabio.2018.05.014 associated with this article can be found, in online version.

Acknowledgments

This work was supported by the Division of Chemical Sciences, Geosciences, and Biosciences, Office of Basic Energy Sciences of the U.S. Department of Energy (Grant DE-FG02-10ER16195). D.J.V. was supported through a National Defense Sciences and Engineering Graduate Fellowship (32CFR168a).

References

[1] R.E. Blankenship, Molecular Mechanisms of Photosynthesis, 2nd ed, Wiley-Blackwell, 2014.
[2] D.J. Vinyard, G.W. Brudvig, Progress toward a molecular mechanism of water oxidation in photosystem II, Annu. Rev. Phys. Chem. 68 (1) (2017) 101–116.
[3] J.-R. Shen, The structure of photosystem II and the mechanism of water oxidation in photosynthesis, Annu. Rev. Plant Biol. 66 (1) (2015) 23–48.
[4] M. Pérez-Navarro, et al., Recent developments in biological water oxidation, Curr. Opin. Chem. Biol. 31 (2016) 113–119.
[5] N. Cox, J. Messinger, Reflections on substrate water and dioxygen formation, Biochim. Biophys. Acta 1827 (8–9) (2013) 1020–1030.
[6] F.M. Ho, S. Styring, Access channels and methanol binding site to the CaMn4 cluster in Photosystem II based on solvent accessibility simulations, with implications for substrate water access, Biochim. Biophys. Acta (BBA) Bioenerg. 1777 (2) (2008) 140–153.
[7] S. Vassiliev, T. Zaraiskaya, D. Bruce, Exploring the energetics of water permeation in photosystem II by multiple steered molecular dynamics simulations, Biochim. Biophys. Acta (BBA) Bioenerg. 1817 (9) (2012) 1671–1678.
[8] M. Askerka, et al., NH3 binding to the S_2 state of the O_2-evolving complex of photosystem II: analogue to H_2O binding during the S2 → S3 transition, Biochemistry 54 (38) (2015) 5783–5786.
[9] F.M. Ho, Structural and mechanistic investigations of photosystem II through computational methods, Biochim. Biophys. Acta (BBA) Bioenerg. 1817 (1) (2012) 106–120.
[10] H. Ishikita, et al., Energetics of a possible proton exit pathway for water oxidation in photosystem II, Biochemistry 45 (7) (2006) 2063–2071.
[11] A.-N. Bondar, H. Dau, Extended protein/water H-bond networks in photosynthetic water oxidation, Biochim. Biophys. Acta (BBA) Bioenerg. 1817 (8) (2012) 1177–1190.
[12] R. Pokhrel, et al., Mutation of lysine 317 in the D2 subunit of photosystem II alters chloride binding and proton transport, Biochemistry 52 (28) (2013) 4758–4773.
[13] K. Linke, F.M. Ho, Water in photosystem II: structural, functional and mechanistic considerations, Biochim. Biophys. Acta (BBA) Bioenerg. 1837 (1) (2014) 14–32.
[14] D.A. Weisz, M.L. Gross, H.B. Pakrasi, Reactive oxygen species leave a damage trail that reveals water channels in Photosystem II, Sci. Adv. 3 (11) (2017).
[15] S. Vassiliev, T. Zaraiskaya, D. Bruce, Molecular dynamics simulations reveal highly permeable oxygen exit channels shared with water uptake channels in photosystem II, Biochim. Biophys. Acta (BBA) Bioenerg. 1827 (10) (2013) 1148–1155.
[16] L. Vogt, et al., Oxygen-evolving complex of Photosystem II: an analysis of second-shell residues and hydrogen-bonding networks, Curr. Opin. Chem. Biol. 25 (2015) 152–158.
[17] D.R. Lide, CRC Handbook of Chemistry and Physics, 88th Ed., CRC Press/Taylor and Francis, Boca Raton, FL, 2008 (Internet Version).
[18] T.H. Nash III, Lichen Biology, Cambridge University Press, Cambridge, 1996.
[19] H. Miyake, et al., Multiple dissipation components of excess light energy in dry lichen revealed by ultrafast fluorescence study at 5 K, Photosynth. Res. 110 (1) (2011) 39.
[20] U. Heber, Photoprotection of green plants: a mechanism of ultra-fast thermal energy dissipation in desiccated lichens, Planta 228 (4) (2008) 641–650.
[21] U. Heber, V. Soni, R.J. Strasser, Photoprotection of reaction centers: thermal dissipation of absorbed light energy vs charge separation in lichens‡, Physiol. Plant. 142 (1) (2011) 65–78.
[22] L. Sass, et al., Changes in photosystem II activity during desiccation and rehydration of the desiccation tolerant lichen *Cladonia convoluta* studied by chlorophyll fluorescence, Photosynth. From Light to Biosphere 4 (1995) 553–556.
[23] O.L. Lange, T.G.A. Green, U. Heber, Hydration-dependent photosynthetic production of lichens: what do laboratory studies tell us about field performance? J. Exp. Bot. 52 (363) (2001) 2033–2042.
[24] G. Ananyev, G.C. Dismukes, How fast can Photosystem II split water? Kinetic performance at high and low frequencies, Photosynth. Res. 84 (1) (2005) 355–365.
[25] V. Ahmadjian, The Lichen Symbiosis, John Wiley & Sons, Inc., New York, 1993.
[26] I.M. Brodo, S.D. Sharnoff, S. Sharnoff, Lichens of North America, Yale University Press, New Haven, 2001.
[27] D.J. Vinyard, G.M. Ananyev, G.C. Dismukes, Photosystem II: the reaction center of oxygenic photosynthesis, Annu. Rev. Biochem. 82 (1) (2013) 577–606.
[28] T.M. Bricker, et al., The extrinsic proteins of Photosystem II, Biochim. Biophys. Acta (BBA) Bioenerg. 1817 (1) (2012) 121–142.
[29] D.J. Vinyard, et al., Thermodynamically accurate modeling of the catalytic cycle of photosynthetic oxygen evolution: a mathematical solution to asymmetric Markov chains, Biochim. Biophys. Acta Bioenerg. 1827 (7) (2013) 861–868.
[30] D.R.J. Kolling, et al., Photosynthetic oxygen evolution is not reversed at high oxygen pressures: mechanistic consequences for the water-oxidizing complex, Biochemistry 48 (6) (2009) 1381–1389.
[31] L.N.M. Duysens, Introduction to (bacterio)chlorophyll emission: a historical perspective, in: J. Amesz Govindjee, D.C. Fork (Eds.), Light Emission by Plants and Bacteria, Acadmic Press, Orlando, Florida, 1986, pp. 3–28.
[32] G. Ananyev, C. Gates, G.C. Dismukes, The oxygen quantum yield in diverse algae and cyanobacteria is controlled by partitioning of flux between linear and cyclic electron flow within photosystem II, Biochim. Biophys. Acta (BBA) Bioenerg. 1857 (9) (2016) 1380–1391.
[33] B. Kok, B. Forbush, M. McGloin, Cooperation of charges in photosynthetic O_2 evolution-I. A linear four step mechanism, Photochem. Photobiol. 11 (6) (1970) 457–475.
[34] J. Cao, Govindjee, Chlorophyll a fluorescence transient as an indicator of active and

inactive Photosystem II in thylakoid membranes, Biochim. Biophys. Acta 1015 (2) (1990) 180–188.
[35] M. Haumann, et al., Photosynthetic oxygen evolution: H/D isotope effects and the coupling between electron and proton transfer during the redox reactions at the oxidizing side of Photosystem II, Photosynth. Res. 51 (3) (1997) 193–208.
[36] R. Mills, Self-diffusion in normal and heavy water in the range 1–45 degrees, J. Phys. Chem. 77 (5) (1973) 685–688.
[37] F.J. Van Eerden, et al., Exchange pathways of plastoquinone and plastoquinol in the photosystem II complex, Nat. Commun. 8 (2017) 15214.
[38] W. Stein, T. Litman, Channels, Carriers, and PUmps, 2nd ed, Academic Press, Orlando, Florida, 2014.
[39] S. Scheiner, M. Cuma, Relative stability of hydrogen and deuterium bonds, J. Am. Chem. Soc. 118 (6) (1996) 1511–1521.
[40] G. Renger, et al., New results on the mechanism of photosynthetic water oxidation, in: G.S. Singhal, et al. (Ed.), Photosynthesis: Molecular Biology and Bioenergetics, Narosa Publishing House, New Dehli, 1989, pp. 355–371.
[41] M. Karge, K.D. Irrgang, G. Renger, Analysis of the reaction coordinate of photosynthetic water oxidation by kinetic measurements of 355 nm absorption changes at different temperatures in photosystem II preparations suspended in either H_2O or D2O, Biochemistry 36 (29) (1997) 8904–8913.
[42] O. Bogershausen, M. Haumann, W. Junge, Photosynthetic oxygen evolution: H/D isotope effects and the coupling between electron and proton transfer during transitions S2 → S3 and S3 → S4 → S0, Ber. Bunsenges. Phys. Chem. 100 (12) (1996) 1987–1992.
[43] P.L. Dilbeck, et al., Perturbing the water cavity surrounding the manganese cluster by mutating the residue D1-valine 185 has a strong effect on the water oxidation mechanism of photosystem II, Biochemistry 52 (39) (2013) 6824–6833.
[44] R. Pokhrel, R.J. Debus, G.W. Brudvig, Probing the effect of mutations of asparagine 181 in the D1 subunit of photosystem II, Biochemistry 54 (8) (2015) 1663–1672.
[45] H. Bao, R.L. Burnap, Structural rearrangements preceding dioxygen formation by the water oxidation complex of photosystem II, Proc. Natl. Acad. Sci. 112 (45) (2015) E6139–E6147.